Theoretical absorption spectrum of the Ar–CO van der Waals complex

Javier López Cacheiro and Berta Fernández[a)]
Department of Physical Chemistry, Faculty of Chemistry, University of Santiago de Compostela, E-15782 Santiago de Compostela, Spain

Thomas Bondo Pedersen and Henrik Koch
Institute of Molecular Science, University of Valencia, E-46100 Burjassot, Valencia, Spain

(Received 12 February 2003; accepted 7 March 2003)

The three-dimensional intermolecular electric dipole moment surface of Ar–CO is calculated at the coupled cluster singles and doubles level of theory with the aug-cc-pVTZ basis set extended with a $3s3p2d1f1g$ set of midbond functions. Using the rovibrational energies and wave functions of our recent study [J. Chem. Phys. **117**, 6562 (2002)], temperature-dependent spectral intensities are evaluated and compared to available experimental data. Based on the theoretical spectrum, alternative assignments of the experimentally observed lines in the fundamental band of CO around 2160 and 2166 cm^{-1} are suggested. © *2003 American Institute of Physics.*
[DOI: 10.1063/1.1570812]

I. INTRODUCTION

The Ar–CO van der Waals complex can be considered a prototype of a weakly bound cluster that consists entirely of heavy atoms. Due to its relative simplicity it has been widely studied both from the experimental[1–19] and the theoretical[20–32] points of view. Because of the very small dipole moment of CO, 0.109 80*D*,[33] Ar–CO is a challenge both from the experimental and the theoretical points of view.

The first experimental observation of the Ar–CO complex was done by De Piante *et al.*[1] and the first detailed studies of the infrared spectrum were reported by McKellar *et al.*[2] They were able to assign six *b*-type transitions (with $\Delta K=\pm 1$) for K values up to 3 in the CO fundamental band. Later Xu *et al.*[7] extended this work to K values up to 6. Havenith *et al.*[4] measured the first excited bending state of Ar–CO, $(\nu_{CO},\nu_{vdW},K)=(1,1,0)$ and König *et al.*[6] detected the (1,1,1) excited bending state that was found to be affected by a strong Coriolis coupling. Later, Xu and McKellar[8] made the first direct observation of the stretching mode. The observation of the higher-lying (1,2,1), (1,3,0), and (1,5,0) states has been recently reported by König and Havenith[10] and Scheele *et al.*[16,17]

With respect to the transitions within the ground state of CO, the first microwave spectrum of Ar–CO was reported by Ogata *et al.*[3] They observed *a*-type transitions (with $\Delta K=0$) for the lowest $K=0$ and 1 levels. Using microwave-millimeter-wave double resonance, Jäger and Gerry[5] were able to observe some *b*-type transitions (with $\Delta K=+1$) and Hepp *et al.*[9] extended these observations. The $K=2\leftarrow 1$ and $3\leftarrow 2$ subbands were measured by Hepp *et al.*[12] by direct absorption of millimeter and submillimeter radiation in a supersonic jet, and by Melnik *et al.*[18] using a fast scan submillimeter-wave spectroscopic technique and a pulsed supersonic jet sample. Recently, using submillimeter-wave absorption spectroscopy in a pulsed supersonic jet, Hepp *et al.*[11] reported the van der Waals bending and Gendriesh *et al.*[14] the van der Waals stretching vibration of Ar–CO.

Many authors have concentrated on calculating accurate intermolecular potential energy surfaces.[23–32] Although fitted to reproduce the lowest excited bending frequency, the best semiempirical potential by Jansen[24,28] allows reproduction of the higher levels. Among the most accurate *ab initio* intermolecular potentials is that of Toczyłowski and Cybulski,[30] obtained for a fixed CO bond distance with the coupled cluster singles and doubles including connected triples corrections method [CCSD(T)] and the augmented correlation consistent polarized triple zeta basis set (aug-cc-pVTZ) extended with two different sets of midbond functions ($3s3p2d2f1g$ and $3s3p2d1f1g$). In Ref. 32 we reported the first three-dimensional *ab initio* intermolecular potential energy surface for the Ar–CO complex using the CCSD(T) method and the augmented correlation consistent polarized quadruple zeta basis set (aug-cc-pVQZ) extended with a set of $3s3p2d1f1g$ midbond functions (denoted 33211). The three-dimensional surface was averaged over the three lowest CO vibrational states and the rovibrational energies were calculated up to 50 cm^{-1} above the ground state. When comparing the results with the available experimental data, 650 observed transitions were reproduced with a rms error of 0.13 cm^{-1}. However, for the experimentally assigned $(2,1)\leftarrow(0,2)$ and $(3,0)\leftarrow(0,0)$ transitions in the CO fundamental band,[10,16] where the states are denoted by the set of (ν_{vdW},K) quantum numbers (see the following for details), large discrepancies were obtained when comparing to the theoretical spectrum. These discrepancies were also found with the previously available intermolecular potential energy surfaces and we were not able to solve them with the theoretical data of our previous work. A complete simulation of the spectrum in this region seems to be needed and therefore, in this work, we proceed with the study of the Ar–CO complex having as main objective the solution of these discrepancies. We carry out the computation of the three-

a)Electronic mail: qfberta@usc.es

dimensional intermolecular electric dipole surface in order to be able to determine the temperature-dependent spectral intensities. Jansen[28] has previously reported theoretical spectral intensities calculated within a Franck–Condon-type approximation where the intermolecular electric dipole contribution is neglected. Such a model is, of course, only valid for transitions involving a change of CO vibrational state.

The paper is organized as follows: In Sec. II we describe the computational details of the evaluation of the intermolecular electric dipole surface and of the transition intensities. In Sec. III we present and discuss the spectroscopic results and Sec. IV contains a summary and concluding remarks.

II. COMPUTATIONAL DETAILS

In Sec. II A we present the computational details of the dipole surface evaluation and in Sec. II B those of the transition intensities.

The Ar–CO internal coordinates are defined as follows: **r** is the vector of length r from C to O, **R** is the van der Waals bond vector of length R from the center of mass of CO to Ar, and θ is the angle between the vectors **r** and **R**. Body-fixed coordinates are used to orientate the dipole moment components. Placing the Ar–CO complex in the xz plane, the body-fixed z axis is chosen parallel to **R** and the x axis perpendicular to z.

A. Dipole surface

In the body-fixed coordinate system, the Cartesian components of the total Ar–CO electric dipole moment can be written as

$$\mu_z(r,R,\theta)=\mu_{\mathrm{CO}}(r)\cos\,\theta+\Delta\mu_z(r,R,\theta), \tag{1}$$

$$\mu_x(r,R,\theta)=\mu_{\mathrm{CO}}(r)\sin\,\theta+\Delta\mu_x(r,R,\theta), \tag{2}$$

where $\mu_{\mathrm{CO}}(r)$ denotes the isolated CO molecular dipole moment curve and $\Delta\mu(r,R,\theta)$ is the intermolecular dipole moment surface.

The intermolecular electric dipole moment is evaluated at a total of 770 geometries[34] using the coupled cluster singles and doubles (CCSD) method and the aug-cc-pVTZ basis set extended with a set of $3s3p2d1f1g$ midbond functions (denoted aug-cc-pVTZ-33211). The midbond functions are well known to improve the property convergence in van der Waals complex calculations (see, e.g., Ref. 35, and references cited therein). The exponents are taken as 0.9, 0.3, and 0.1 for the s and the p functions, 0.6 and 0.2 for the d, and 0.3 for the f and the g functions. The functions are located in the middle of the van der Waals bond. Using the DALTON program,[36,37] the dipole moments are calculated with frozen core orbitals and without orbital relaxation of the coupled cluster density in the property evaluation. The counterpoise corrected results are given in Ref. 34.

The intermolecular electric dipole moment points are fitted to an analytic function. In the above-mentioned body-fixed coordinates the dipole moment is expressed as[38]

$$\Delta\mu_z(r,R,\theta)=\sum_{\lambda=0}^{\infty} C_{\lambda,0}(r,R)P_{\lambda 0}(\theta), \tag{3}$$

$$\Delta\mu_x(r,R,\theta)=\sum_{\lambda=1}^{\infty} C_{\lambda,1}(r,R)P_{\lambda 1}(\theta) \tag{4}$$

in terms of the associated Legendre functions. The Legendre expansions are truncated in $\lambda=6$ for μ_z and $\lambda=5$ for μ_x. The following analytic expressions are used for the $C_{\lambda,\gamma}$ coefficients ($\gamma=0,1$),

$$C_{\lambda,\gamma}=\left(\sum_{n=0}^{3} b_{n,\lambda,\gamma}R^n\right)e^{-B_{\lambda,\gamma}R}, \tag{5}$$

$$b_{n,\lambda,\gamma}=\sum_{m=0}^{2} a_{m,n,\lambda,\gamma}(r-r_e)^m, \tag{6}$$

$$B_{\lambda,\gamma}=\sum_{m=0}^{2} c_{m,\lambda,\gamma}(r-r_e)^m, \tag{7}$$

with $r_e=2.132$ bohr. For CO distances less than 1.19 Å, the fit has a rms error of 5×10^{-5} a.u. in the $\Delta\mu_x$ component and 1×10^{-4} a.u. in $\Delta\mu_z$. The parameters obtained are given in Ref. 34. For checking the quality of the fit 18 additional points are calculated. The fitted surface describes these new points with maximum errors of 3×10^{-4} a.u. (2×10^{-3} a.u.) for $\Delta\mu_x$ ($\Delta\mu_z$). The intermolecular dipole surface is highly anisotropic, as can be seen in Figs. 1 and 2 where contour diagrams of the $\Delta\mu_x$ and $\Delta\mu_z$ components are given for $r=r_e$.

B. Transition intensities

In our previous work we evaluated the rovibrational energy levels of the Ar–CO complex within the vibrationally adiabatic approximation.[32] The Born–Oppenheimer Schrödinger equation for nuclear motion was solved, using the appropriately averaged potential and rotational constants for each CO vibrational state, to obtain the rovibrational energies and wave functions of the van der Waals modes. The total energy of a given state is then given by

$$E^{J,p}_{\nu_{\mathrm{CO}},\nu_{\mathrm{vdW}},K}=E_{\nu_{\mathrm{CO}}}+\Delta E^{J,p}_{\nu_{\mathrm{CO}},\nu_{\mathrm{vdW}},K}, \tag{8}$$

where $E_{\nu_{\mathrm{CO}}}$ is the CO vibrational energy and $\Delta E^{J,p}_{\nu_{\mathrm{CO}},\nu_{\mathrm{vdW}},K}$ is the van der Waals mode energy. The quantum numbers ν_{CO} and ν_{vdW} label the intra- and intermolecular vibrational modes, respectively, and the approximate quantum number K (equal to K_a in the usual $J_{K_aK_c}$ notation of asymmetric rotors) represents the projection of the total angular momentum on the intermolecular a axis. J is the total angular momentum quantum number and p the parity. Transition frequencies are obtained as energy differences. Using the corresponding eigenfunctions and the electric dipole moment surface, rovibrational transition intensities can be evaluated.

The integrated absorption coefficient can be derived within the vibrationally adiabatic approximation as

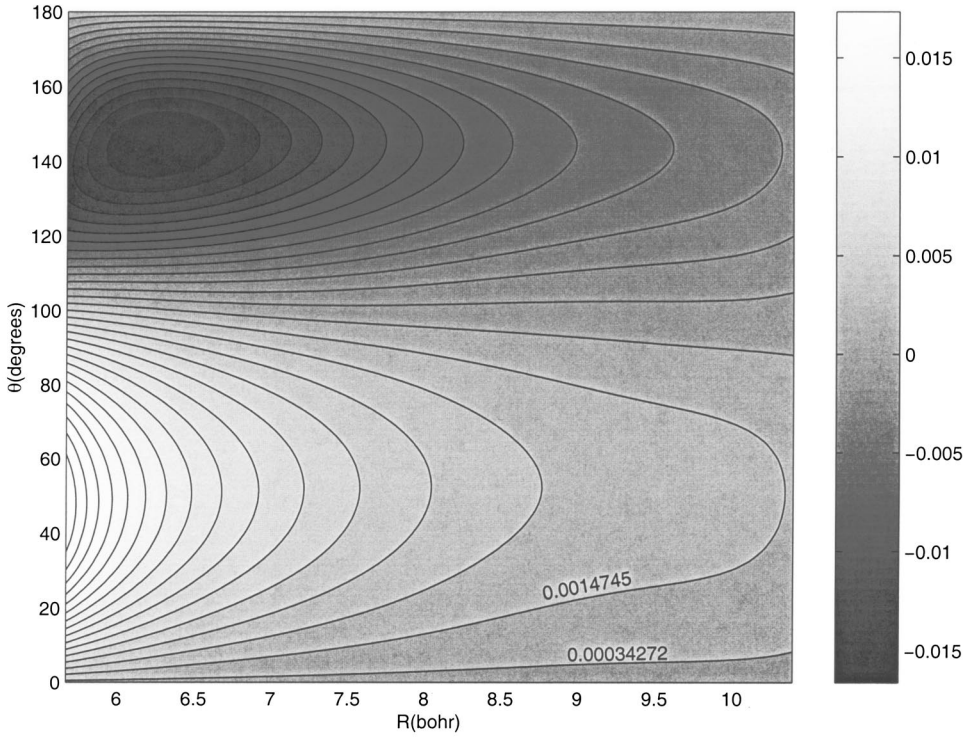

FIG. 1. Contour diagram for the $\Delta\mu_x$ component of the dipole moment in a.u. at $r=2.132$ bohr, the increment between subsequent curves is 0.001 130 1 a.u.

$$\int_{\text{line } i\to f}\kappa(\nu)d\nu=\frac{8\pi^3}{3ch}\left(\frac{N_f}{g_f}-\frac{N_i}{g_i}\right)\omega_{i,f}\sum_{n,m}|\langle f_m|\mu|i_n\rangle|^2, \tag{9}$$

where N_f and N_i represent the density of molecules in the final and initial states, respectively, for which a Boltzmann distribution is assumed. The degeneracies of the final and initial levels are denoted g_f and g_i. The indices n and m run over the degenerate states of the corresponding level, and $\omega_{i,f}$ represents the transition frequency of the transition from the state described by the wave function i_n to that characterized by f_m. The total dipole moment vector μ is calculated by adding the empirical CO dipole moment curve of Ogilvie *et al.*[39] to the fitted intermolecular potential according to Eqs. (1) and (2).

The dipole matrix elements are evaluated as

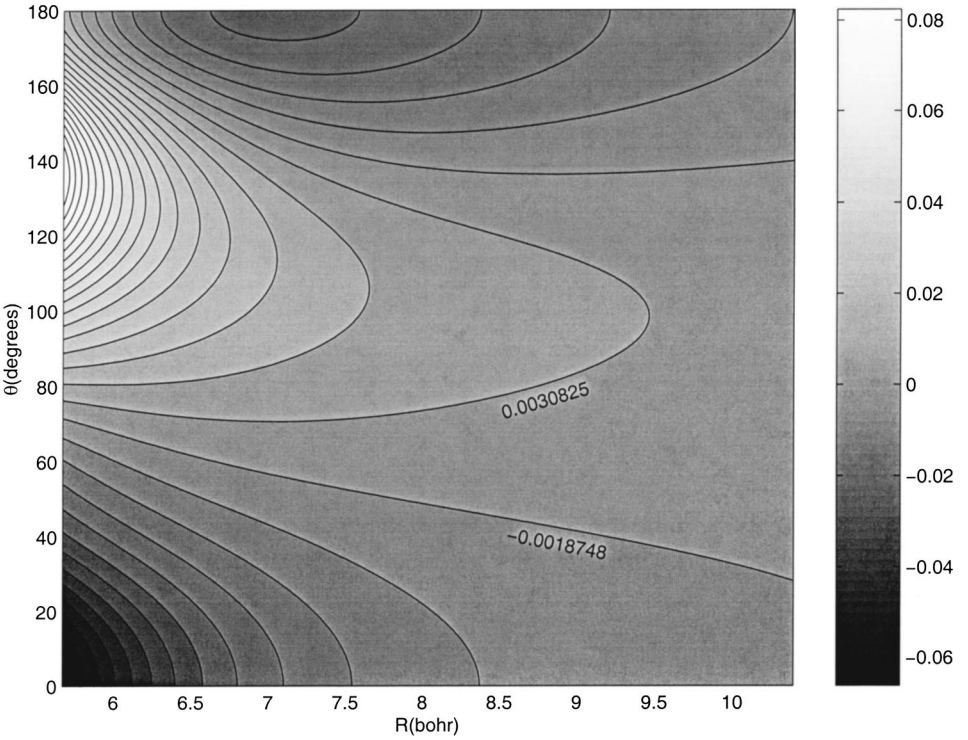

FIG. 2. Contour diagram for the $\Delta\mu_z$ component of the dipole moment in a.u. at $r=2.132$ bohr, the increment between subsequent curves is 0.001 130 1 a.u.

$$\langle f_m|\mu_z|i_n\rangle=\langle J',p',\nu'_{\rm vdW},K'|\mu_{\rm CO}^{\nu'_{\rm CO}\nu_{\rm CO}}\cos\,\theta + \Delta\mu_z^{\nu'_{\rm CO}\nu_{\rm CO}}(R,\theta)|J,p,\nu_{\rm vdW},K\rangle, \quad (10)$$

$$\langle f_m|\mu_x|i_n\rangle=\langle J',p',\nu'_{\rm vdW},K'|\mu_{\rm CO}^{\nu'_{\rm CO}\nu_{\rm CO}}\sin\,\theta + \Delta\mu_x^{\nu'_{\rm CO}\nu_{\rm CO}}(R,\theta)|J,p,\nu_{\rm vdW},K\rangle, \quad (11)$$

where $\mu_{\rm CO}^{\nu'_{\rm CO}\nu_{\rm CO}}$ and $\Delta\mu^{\nu'_{\rm CO}\nu_{\rm CO}}(R,\theta)$ are matrix elements over the CO vibrational states. It is implicitly understood that the quantum numbers in the bra (ket) belong to the final (initial) CO vibrational level $\nu'_{\rm CO}(\nu_{\rm CO})$.

Following the same procedures as that used in the evaluation of the intermolecular potential energy surface,[32] the vibrational matrix elements, $\Delta\mu^{\nu'_{\rm CO}\nu_{\rm CO}}(R,\theta)$, may be calculated with the aid of a Taylor expansion of $\Delta\mu(r,R,\theta)$ about r_e as

$$\Delta\mu^{\nu'_{\rm CO}\nu_{\rm CO}}(R,\theta)=\langle\tilde{G}_{\nu'_{\rm CO}}|\Delta\mu(r,R,\theta)|\tilde{G}_{\nu_{\rm CO}}\rangle = \sum_{k=0}^{k_{\max}}\frac{1}{k!}\left(\frac{\partial^k\Delta\mu(r,R,\theta)}{\partial r^k}\right)_{r=r_e} \times\langle\tilde{G}_{\nu'_{\rm CO}}|(r-r_e)^k|\tilde{G}_{\nu_{\rm CO}}\rangle, \quad (12)$$

where the CO vibrational eigenfunctions $\tilde{G}_{\nu_{\rm CO}}(r)$ are determined from the potential curve $V_{\rm CO}(r)$ for zero angular momentum. As in our previous work,[32] we deploy the empirical potential curve of Huxley and Murrel[40] (with $r_e=2.132$ bohr) for calculating $\tilde{G}_{\nu_{\rm CO}}(r)$, $\nu_{\rm CO}=0,1$, and the matrix elements of $(r-r_e)^k$ are evaluated using the VIBROT module of the MOLCAS program suite.[41] The Taylor series is truncated at $k_{\max}=8$, as the contributions in Eq. (12) for larger k are less than 10^{-6} a.u. in the case of $\Delta\mu_x$ and less than 10^{-4} a.u. in the case of $\Delta\mu_z$, lower in both cases than the rms errors of the corresponding fits.

The dipole matrix elements, Eqs. (10) and (11), are calculated with a locally modified version of the TRIATOM program[42] using the rovibrational energies and wave functions of Ref. 32. A comparison of the CO and intermolecular contributions to the dipole moment components is shown in Figs. 3 and 4 for the CO fundamental band. The intermolecular contribution is clearly negligible compared to the CO contribution, thus justifying the approximation employed by Jansen.[28]

Most of the experimental data available for the infrared spectra have been obtained using supersonic jet spectrometers with a rotational temperature of the jet of about 10 K. In some cases a cooled (~50 K) long-path cell coupled with a Fourier transform spectrometer or with a tunable diode laser was used as a complementary technique. We therefore evaluate the infrared spectral intensities at 10 and 50 K.

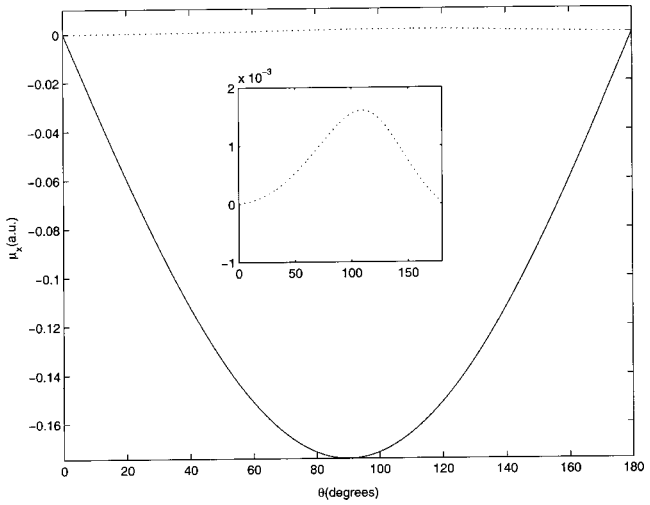

FIG. 3. Vibrational matrix element contributions to the total x component of the dipole matrix element $\mu_x^{10}=\mu_{\rm CO}^{10}\sin\theta+\Delta\mu_x^{10}$ at $R=3.72$ Å. The solid line represents the $\mu_{\rm CO}^{10}\sin\theta$ contribution and the dashed line the $\Delta\mu_x^{10}$ contribution.

III. RESULTS

In Sec. III A we present the pure van der Waals spectrum within the vibrational ground state of CO, while the intermolecular lines within the CO fundamental band are discussed in Sec. III B.

For labeling the transitions we use the notation $(\nu'_{\rm vdW},K')\leftarrow(\nu_{\rm vdW},K)$, the initial and final vibrational states of CO being implicitly understood. The usual P,Q,R notation is employed to denote the $\Delta J=-1,0,1$ rotational branches, respectively. Unless stated otherwise, for transitions involving asymmetry split states, the $P1,Q1,R1$ ($P2,Q2,R2$) branches are those involving the lower (higher) asymmetry component of the initial state.

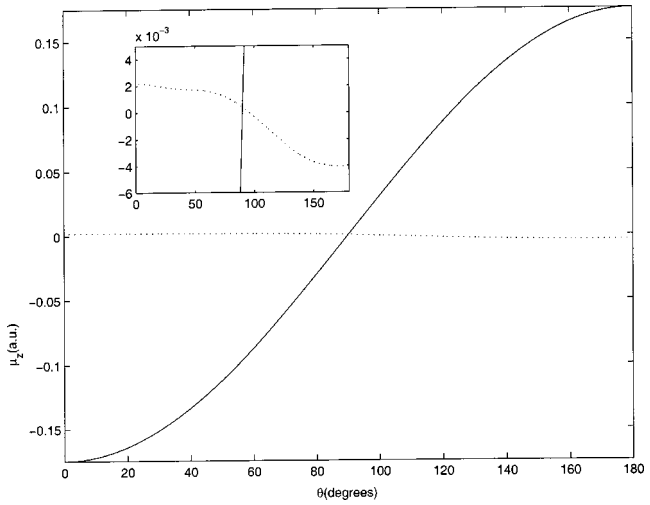

FIG. 4. Vibrational matrix element contributions to the total z component dipole matrix element $\mu_z^{10}=\mu_{\rm CO}^{10}\cos\theta+\Delta\mu_z^{10}$ at $R=3.72$ Å. The solid line represents the $\mu_{\rm CO}^{10}\cos\theta$ contribution and the dashed line the $\Delta\mu_z^{10}$ contribution.

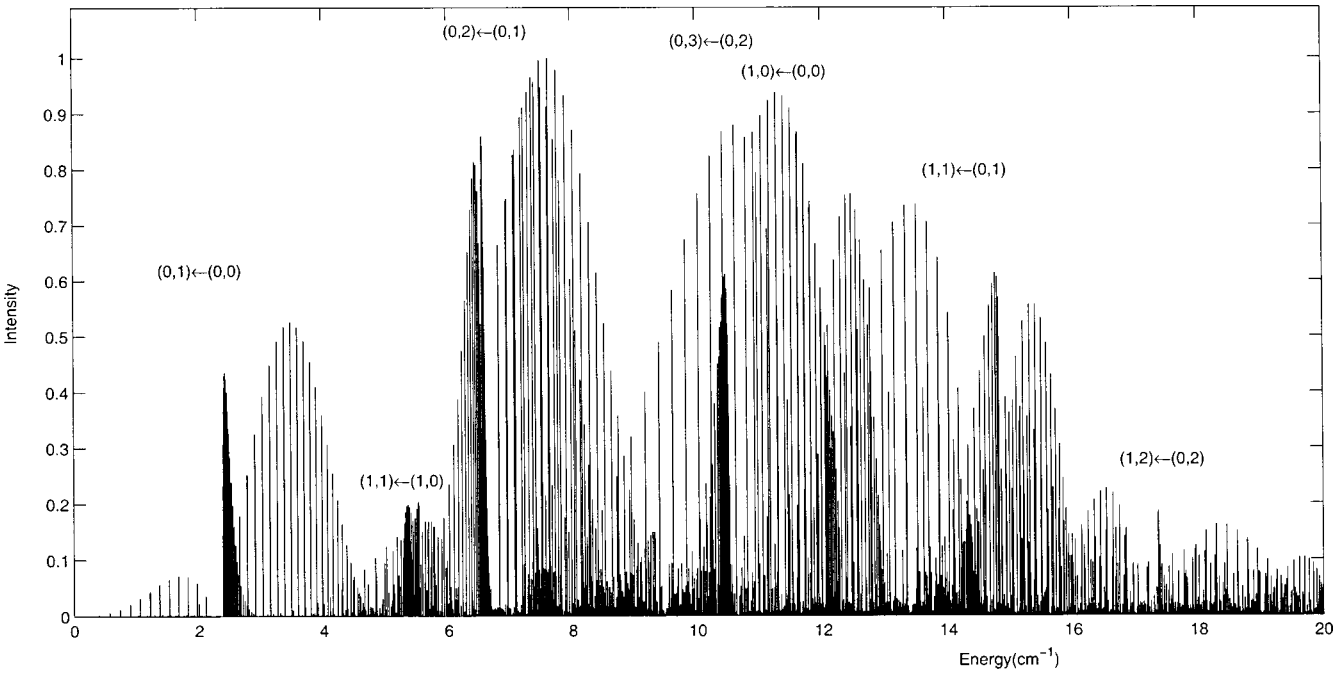

FIG. 5. Microwave, millimeter- and submillimeter-wave absorption spectrum at 10 K.

A. van der Waals spectrum in the CO vibrational ground state

The results for the CO vibrational ground state spectrum (transitions characterized by $\nu'_{CO}=\nu_{CO}=0$) are presented in Figs. 5–7. In all figures, the absorption intensities are plotted relative to the most intense line, namely the $R1(7)$ line corresponding to the $(0,2)\leftarrow(0,1)$ transition.

Figure 5 shows the van der Waals rovibrational spectrum of Ar–CO in the CO ground state at 10 K. Comparing with Fig. 6, which contains only transitions within the van der Waals ground state, $\nu_{vdW}=\nu'_{vdW}=0$ and $\Delta K=1$, it can be seen that most of the intense bands in the spectrum are due to $\Delta K=1$ transitions. In general, these transitions are mainly characterized by strong R branches, relatively broad Q branches, and comparatively very weak P branches. The $(0,1)\leftarrow(0,0)$ transition was first measured by Jäger and Gerry[5] using a double resonance technique and, more recently, Hepp *et al.*[9] extended the previous work using a combination of millimeter-wave absorption spectroscopy and supersonic jet expansion. The weak P branch of this transition remains unmeasured. The P and R branches of the $(0,2)\leftarrow(0,1)$ transition have been measured by Hepp *et al.*[12] using direct absorption of millimeter radiation in a supersonic jet. Later, Melnik *et al.*[18] also observed some lines of the $Q1$ branch of the same transition using a combination of a fast submillimeter-wave spectroscopic technique and a pulsed supersonic jet sample. The Q and R branches of the $(0,3)\leftarrow(0,2)$ transition were measured by Hepp *et al.*[9] In the

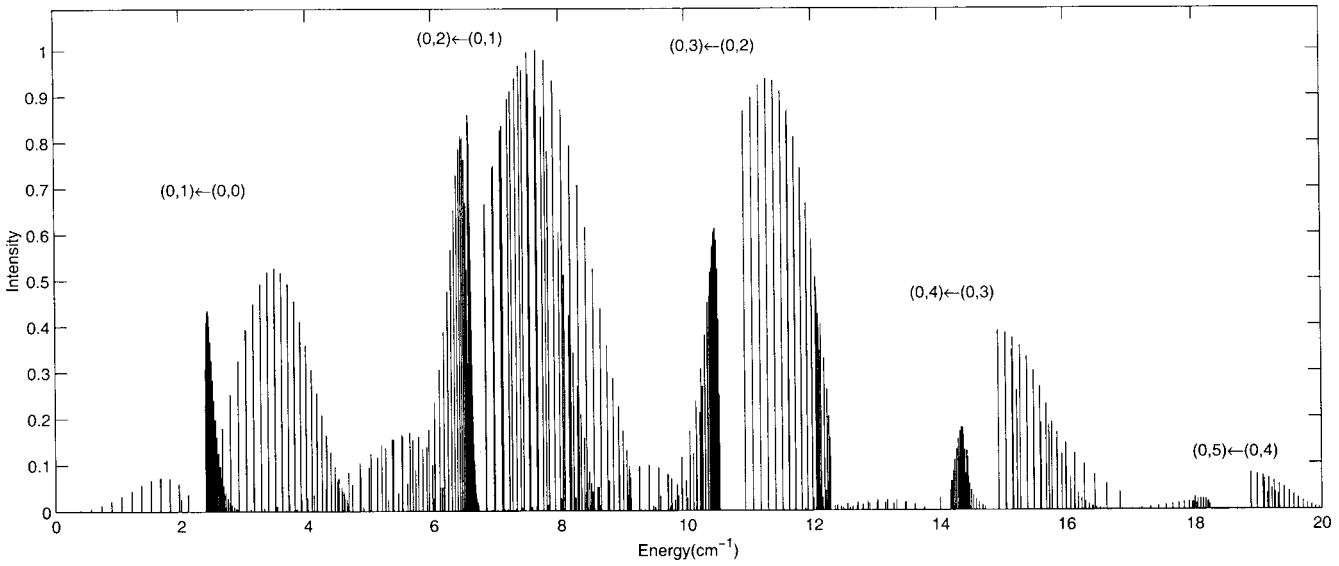

FIG. 6. Microwave, millimeter- and submillimeter-wave absorption spectrum at 10 K. Transitions with $\nu_{vdW}=\nu'_{vdW}=0$ and $\Delta K=1$.

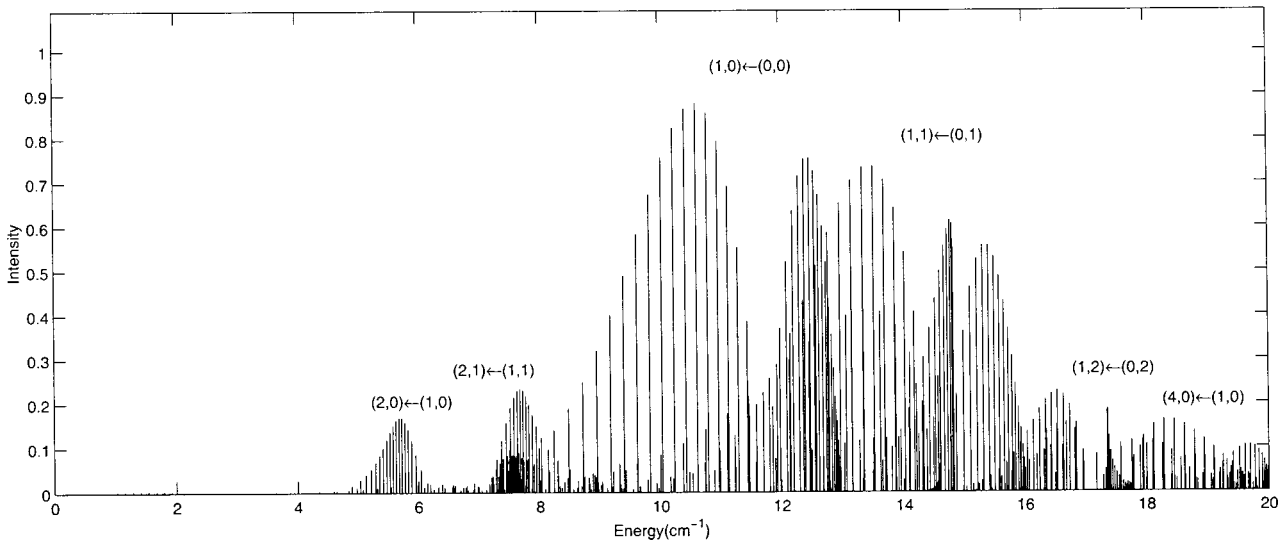

FIG. 7. Microwave, millimeter- and submillimeter-wave absorption spectrum at 10 K. Transitions with $\Delta K=0$.

case of the relatively intense $(0,4)\leftarrow(0,3)$ transition only the $R(3)$ lines have been experimentally reported.[14]

Other relatively intense transitions are those with $\Delta K=0$, in particular those from the ground ($\nu_{\mathrm{vdW}}=0$) to the first excited van der Waals state ($\nu'_{\mathrm{vdW}}=1$), see Fig. 7 where only transitions with $\Delta K=0$ are plotted. The P branch of the $(1,0)\leftarrow(0,0)$ transition is more intense and much broader than the R branch. In the case of the $(1,1)\leftarrow(0,1)$ transition the P branches are also the most intense. The structure of this transition is very complex with a very broad $Q1$ branch and overlap between P and R branches. The $(1,0)\leftarrow(0,0)$ transition was measured by Hepp *et al.*[11] using submillimeter-wave spectroscopy in a pulsed supersonic jet. Recently, Hepp *et al.*[14] measured the weak $(2,0)\leftarrow(0,0)$ transition that is located in the 16–20 cm^{-1} frequency range. In our case this transition is located in the same energy range but it is very weak with intensities about 100 times weaker than those of the $(1,0)\leftarrow(0,0)$ transition.

B. van der Waals spectrum in the CO fundamental band

1. General features

The results for the spectrum embedded in the CO fundamental band (transitions characterized by $\nu'_{\mathrm{CO}}=1$ and $\nu_{\mathrm{CO}}=0$) are presented in Figs. 8–13, and in Tables I and II. In all figures, the absorption intensities are plotted relative to the most intense line, namely the $Q(7)$ line corresponding to the $(0,1)\leftarrow(0,0)$ transition.

Figure 8 shows the infrared spectrum at 10 K. The difference in intensity between the P and R branches reflects the fact that Ar–CO is an intermediate case between the rigid

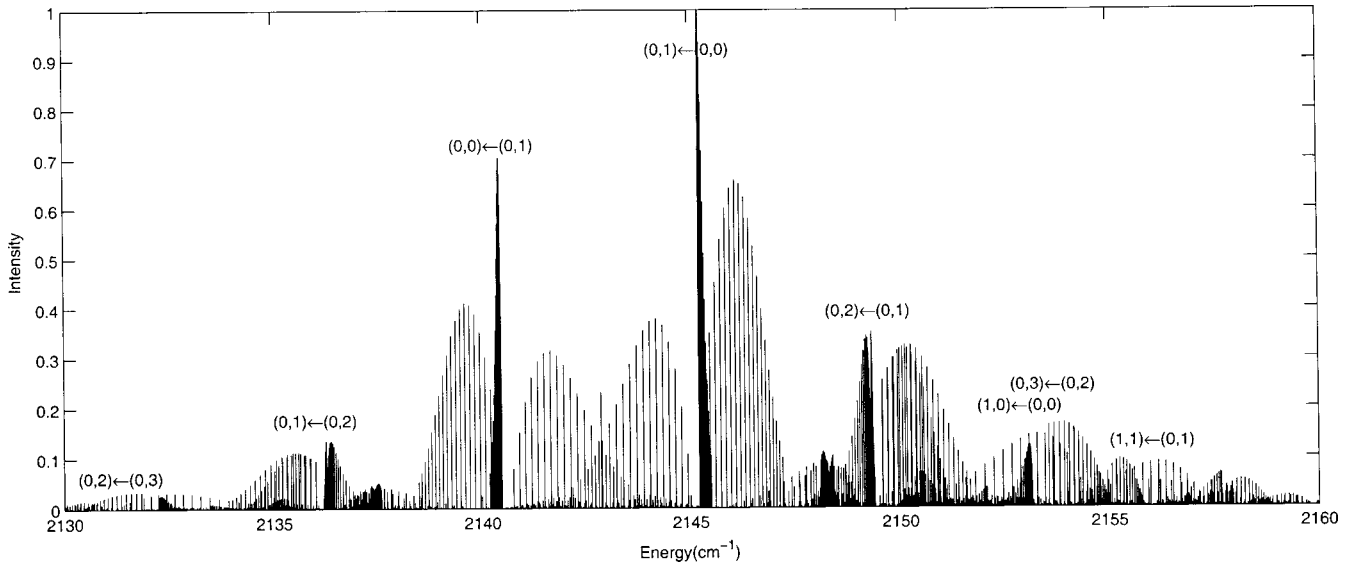

FIG. 8. Infrared absorption spectrum at 10 K.

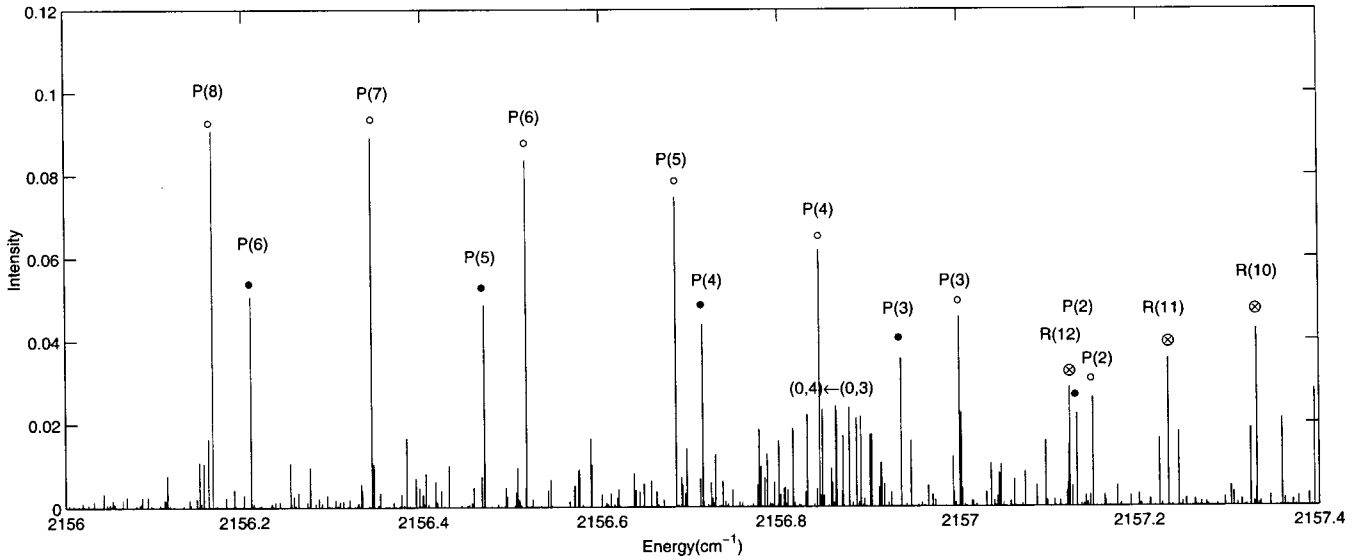

FIG. 9. (1,1)←(0,1): (○) $P2$ branch, (●) $P1$ branch, (⊗) $R1$ branch. The Q branches of the (0,4)←(0,3) transition are observed around 2156.8 cm^{-1}.

rotor and the free rotor limit. In the case of a rigid rotor the P and R branches would have equal intensity while in the free rotor limit the branch with $\Delta J=-\Delta K$ is expected to be weaker. In agreement with experiment, at this temperature the most intense lines of the spectrum correspond to van der Waals ground state bands ($\nu'_{\mathrm{vdW}}=\nu_{\mathrm{vdW}}=0$). The $K=1\leftarrow 0$ and $0\leftarrow 1$ bands, located around 2145 and 2140 cm^{-1}, respectively, are the most intense. The $K=2\leftarrow 1$ and $1\leftarrow 2$ bands are the next strongest features in the spectrum. Initially no lines had been observed experimentally for the weaker P branches of the $K=2\leftarrow 1$ and the R branches of its mirror image $K=1\leftarrow 2$.[2] According to our spectrum these branches have an intensity five times smaller than their respective Q branches. They were observed for the first time in Ref. 8. McKellar *et al.*[2] neither observed the P branches of the $K=3\leftarrow 2$ nor the Q and R branches of the $K=2\leftarrow 3$ transitions. According to our results, the intensity of the P branches of the $K=3\leftarrow 2$ transition is around ten times smaller than that of the more intense R branches. The R branches of the $K=2\leftarrow 3$ transition are very weak compared to the P branches, but the narrow Q branches of this transition, located around 2132.3 cm^{-1}, are almost as intense as the P branches.

Among the transitions involving excited van der Waals states the most intense are the parallel transitions. The (1,0)←(0,0) transition is the most intense and it was measured by Havenith *et al.*[4] The (1,1)←(0,1) is also relatively intense, and suffers a strong Coriolis interaction, reflected in the high asymmetry splitting and in the fact that the P branches are stronger than the R branches. The P and R branches were measured first by König *et al.*[6] and some lines of the much weaker $Q2$ branch later by Xu *et al.*[8] The $Q1$ branch, located around 2157.4 cm^{-1}, whose maximum intensity is similar to that of the $Q2$ branch, is still unobserved, possibly because the intensity falls off with J much faster than that in the $Q2$ branch and therefore the only lines whose

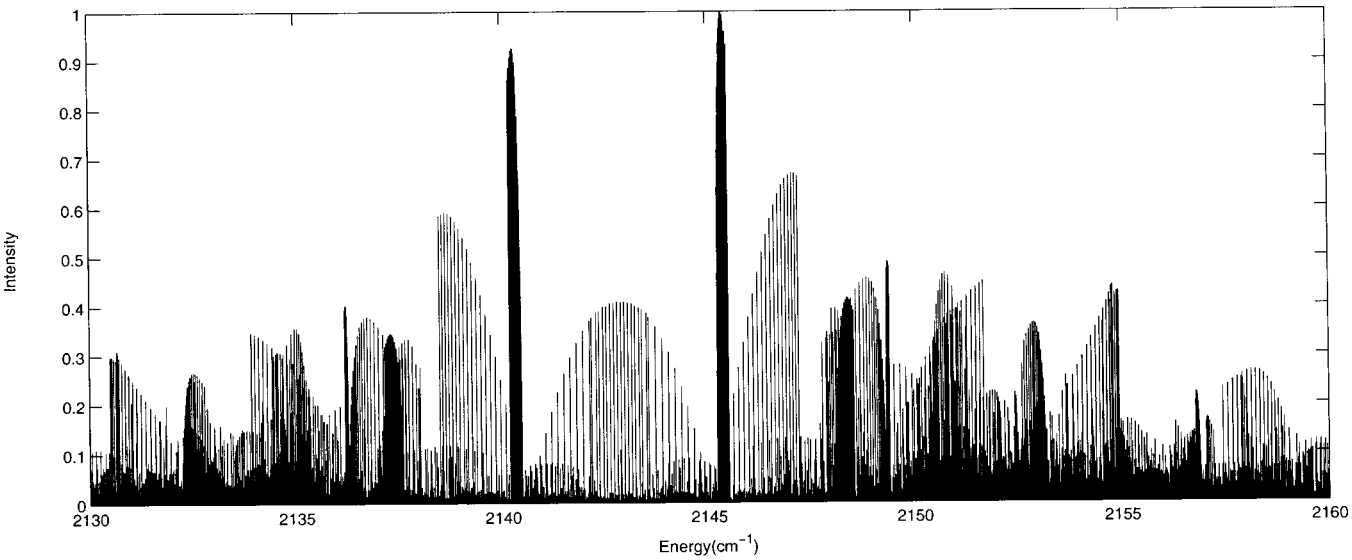

FIG. 10. Infrared absorption spectrum at 50 K.

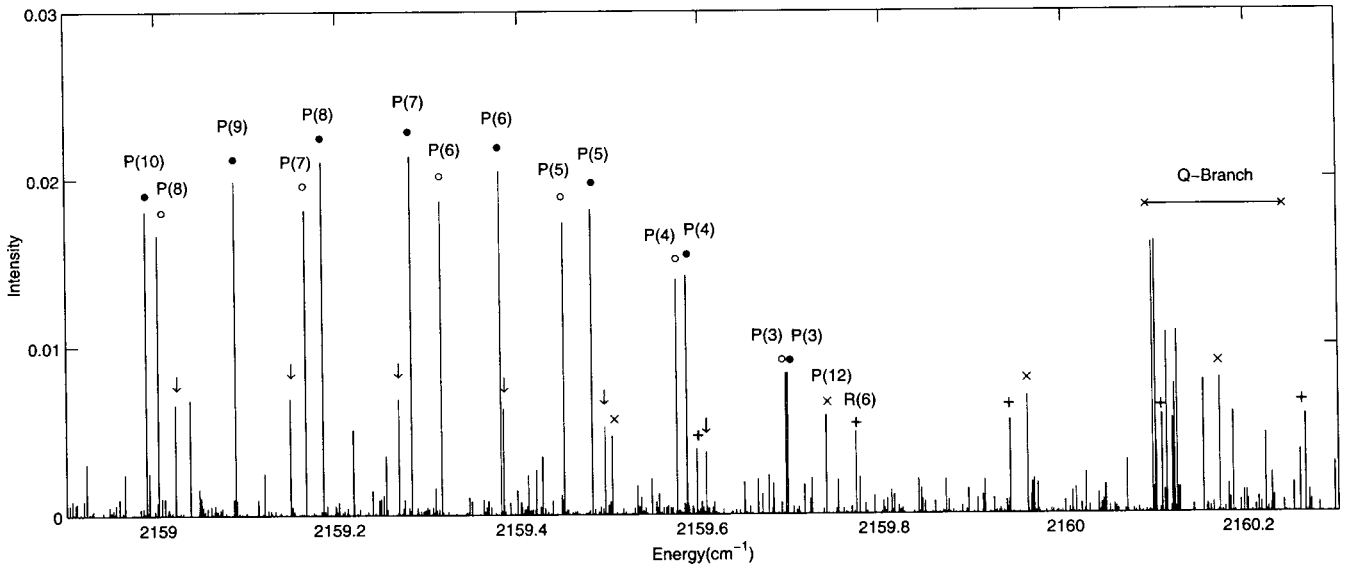

FIG. 11. (1,2)←(0,2): (●) $P2$ branch, (○) $P1$ branch, the Q branches are around 2160.1 cm^{-1}; (×) (4,0)←(1,0) P branch; (+) (2,0)←(0,1) R branch; (↓) (3,0)←(0,2) P branch.

relative intensity is higher than 0.01 are the $Q1(1)$ and the $Q1(2)$. Very good agreement between theory and experiment is seen by comparing Fig. 9 with Fig. 2 of Ref. 6, depicting the (1,1)←(0,1) and (0,4)←(0,3) transitions in the 2157 cm^{-1} region.

Xu and McKellar[8] also observed the R branch of the (1,0)←(2,0), the P branch of its mirror image (2,0)←(1,0), the P branch of the (2,0)←(0,1), the P and Q branches of the (1,0)←(1,1), and the Q and R branches of its mirror image (1,1)←(1,0). For these lines we find that the unmeasured branches are the weakest in each transition (in general one order of magnitude lower than those measured).

The theoretical and experimental spectra thus share important general features, giving us confidence in the reliability of our spectrum when analyzing the experimental assignments of the (2,1)←(0,2) and (3,0)←(0,0) transitions (see the following).

Figure 10 shows the spectrum at 50 K. Like at 10 K the most intense lines of the spectrum correspond to van der Waals ground state bands, and as expected at this temperature it is much easier to observe transitions involving initial excited van der Waals states or states with higher K values. The much higher relative intensities of the lines corresponding to high J values can also be observed.

2. The 2160 and 2166 cm^{-1} regions

In Ref. 32 we were able to reproduce the experimentally observed transition frequencies (about 650 lines) with a rms

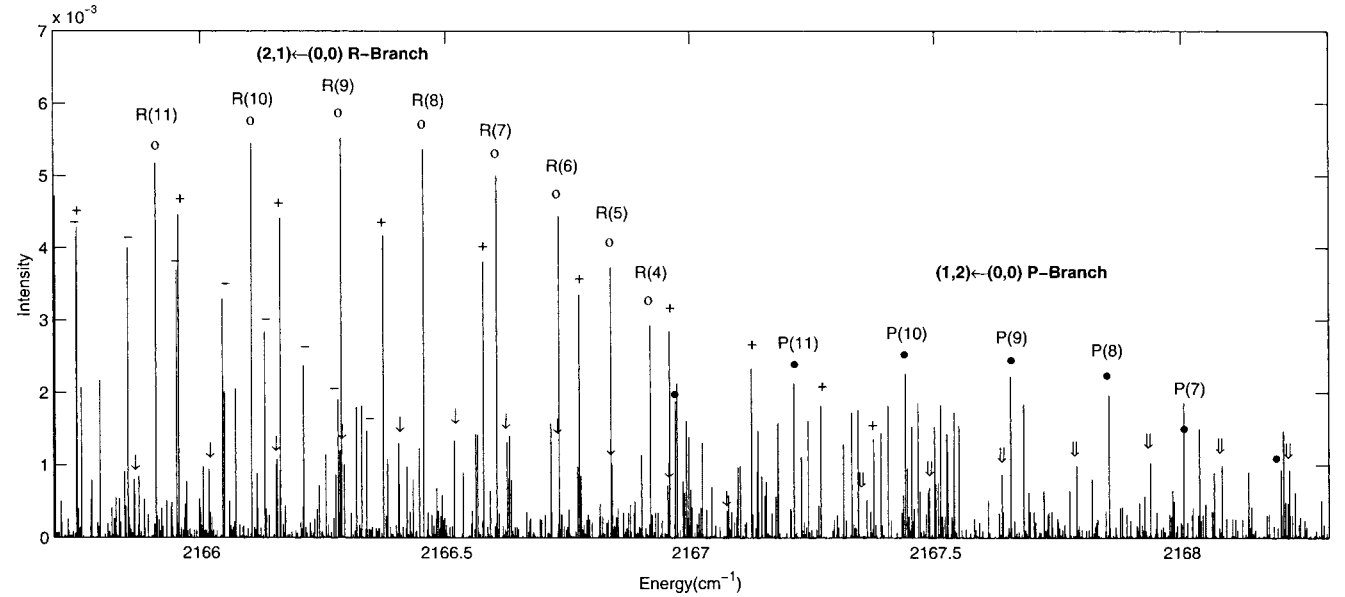

FIG. 12. (○) R branch of the (2,1)←(0,0); (●) P branch of the (1,2)←(0,0); (↓) and (⇓) represent the $P(11)$-$P(1)$ and $R(0)$-$R(6)$ branches of the (5,0)←(1,0), respectively; (+) and (−) indicate the $R1$ and $R2$ branches of the (4,1)←(1,1) transition, respectively; the lines observed around 2167.5 cm^{-1} belong to the R branches of the (1,2)←(0,0) transition.

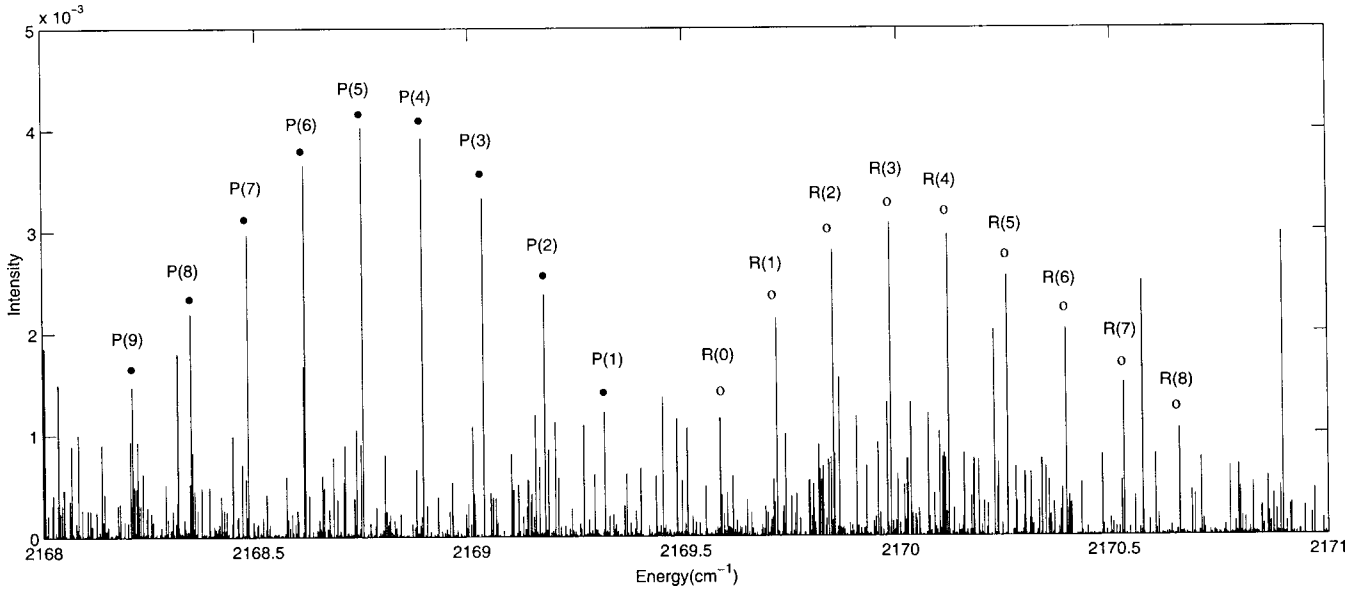

FIG. 13. (3,0)←(0,0): (○) *P* branch; (●) *R* branch.

error of 0.13 cm^{-1}, excluding those transitions involving states around 25 cm^{-1} above the van der Waals ground state for $\nu_{CO}=1$. For transitions involving these states errors as large as 3 cm^{-1} were found. This value is much larger than the overall precision obtained in the description of all other observed transitions, including the (5,0)←(1,0) transition that was measured in the same energy region as the (3,0)←(0,0) and involves an even higher van der Waals state. In this section we attempt to solve these discrepancies based on the *ab initio* intensity data.

The (2,1)←(0,2) transition was experimentally observed around 2160 cm^{-1} by König and Havenith.[10] In the theoretical spectrum the (1,2)←(0,2) transition is the most intense in this region (see Fig. 11) with intensities around one order of magnitude smaller than those of the (1,1)←(0,1) (see Fig. 9). The *Q* branches of the (1,2)←(0,2) transition are close in intensity to the *P* branches even though the *Q* branches would not be allowed in the case of a totally symmetric rotor. The *R* branches, located in the 2161–2163 cm^{-1} range, are the least intense and the broadest. The *P* branches of the (3,0)←(0,2) (around 2159.2 cm^{-1}) and the (4,0)←(1,0) (around 2160.5 cm^{-1}) transitions are located in the 2159–2162 cm^{-1} region.

Based on an analysis of combination differences and rotational constants, König and Havenith[10] assigned the initial state of the transitions observed around 2160 cm^{-1} to the (0,2) level. The final state was subsequently deduced as (2,1) since *P* lines were observed for $J=2$, thus forcing the final level to have $K=1$. Comparing Fig. 11 with the measurements of König and Havenith[10] in this region, the degenerate $P(2)$ lines experimentally observed at 2159.8139 cm^{-1} might correspond to the $P(12)$ line of the (4,0)←(1,0) transition (theoretically at 2159.737 cm^{-1}) or the $R(6)$ line of the (2,0)←(0,1) transition (theoretically at 2159.770 cm^{-1}). As the initial state of the transition is (0,2), the lack of $P(2)$ lines allows us to reassign the final level to (1,2). Thus reassigned, Table I reveals excellent agreement between theory and experiment in the 2160 cm^{-1} region.

The other transition with surprisingly large discrepancy between theory and experiment is the (3,0)←(0,0) that was

TABLE I. Error statistics (Δ_{min} and Δ_{max} are absolute minimum and maximum errors, and Δ_{rms} the rms error; in cm^{-1}) for transitions in the CO fundamental band; *N* is the number of lines included from a given branch. Experimental results are taken from the indicated reference.

Transition	Reference	Branch[a]	*N*	Δ_{min}	Δ_{max}	Δ_{rms}
(1,1,2)←(0,0,2)[b]	10	P1	8	0.0015	0.0070	0.0038
		P2	8	0.0038	0.0456	0.0271
		Q1	8	0.0049	0.0198	0.0127
		Q2	8	0.0072	0.0581	0.0351
		R1	7	0.0147	0.0304	0.0210
		R2	7	0.0165	0.0704	0.0456
(1,2,1)←(0,0,0)[c]	16	R	10	0.3643	0.7335	0.6420
(1,1,2)←(0,0,0)[d]	16	P	5	0.0756	1.2538	0.7932

[a]Suffix 1 (2) signifies that the transitions end in the lower-energy (higher-energy) *K* state.
[b]Original experimental assignment: (1,2,1)←(0,0,2).
[c]Original experimental assignment: (1,3,0)←(0,0,0), *P* branch.
[d]Original experimental assignment: (1,3,0)←(0,0,0), *R* branch.

TABLE II. Rotational constants (in cm^{-1}) for all states up to 40 cm^{-1} above the $\nu_{CO}=1$ van der Waals ground state. The last column contains the rms errors (in cm^{-1}) of the fits.

(ν_{CO},ν_{vdW},K)	B (expt.)	B (theory)	Δ_{rms}
(1,5,0)	0.0645	0.0689[d]	2×10^{-4}
		0.0678[e]	5×10^{-3}
(1,3,1)		0.0615[d]	7×10^{-4}
		0.0611[e]	2×10^{-3}
(1,2,2)		0.0538[d]	5×10^{-4}
		0.0538[e]	7×10^{-4}
(1,4,0)		0.0615[d]	5×10^{-6}
		0.0616[e]	1×10^{-4}
(1,3,0)	0.0747	0.0533[d]	5×10^{-2}
		0.0750[e]	1×10^{-1}
(1,1,2)		0.0807[d]	7×10^{-2}
		0.0656[e]	8×10^{-2}
(1,1,2)e		0.0901[c]	9×10^{-2}
		0.0603[b]	1×10^{-1}
(1,1,2)f		0.0714[c]	4×10^{-5}
		0.0709[b]	2×10^{-3}
(1,2,1)	0.0709	0.0521[d]	3×10^{-4}
		0.0531[e]	4×10^{-3}
(1,2,1)e		0.0466[c]	3×10^{-4}
		0.0482[b]	6×10^{-3}
(1,2,1)f		0.0576[c]	5×10^{-5}
		0.0581[b]	2×10^{-3}
(1,2,0)	0.0619	0.0611[a]	7×10^{-6}
(1,1,1)e	0.0652	0.0647[a]	7×10^{-6}
(1,1,1)f	0.0669	0.0663[b]	2×10^{-5}
(1,1,0)	0.0653	0.0646[d]	9×10^{-8}
		0.0646[b]	8×10^{-7}

[a]Fitted using the expression for two Coriolis coupled states obtained in Ref. 6.
[b]$E=\sigma+B[J(J+1)-K^2]-D[J(J+1)-K^2]^2$.
[c]$E=\sigma+B[J(J+1)-K^2]-D[J(J+1)-K^2]^2+H[J(J+1)-K^2]^3+L[J(J+1)-K^2]^4$.
[d]Equation (13) in the text.
[e]$E=\sigma+B[J(J+1)-K^2]-D[J(J+1)-K^2]^2\pm\frac{1}{2}S$.

measured by Scheele *et al.*[16] in the region around 2166 cm^{-1}. The predicted intensities in this region of the spectrum, Fig. 12, are about an order of magnitude smaller than those in Fig. 11.

According to Fig. 2 of Ref. 16, the most intense lines around 2166.0 cm^{-1} correspond to the P branch of the (3,0)←(0,0) transition, and some weaker lines are assigned to the (5,0)←(1,0) P branch around 2166.3 cm^{-1}. According to Fig. 1 of Ref. 17, the most intense lines in the 2167.7 cm^{-1} region correspond to the R branch of the (3,0)←(0,0) transition. In the same region some weaker lines are assigned to the (5,0)←(1,0) P branch, and the R branch of the (5,0)←(1,0) transition appears around 2168 cm^{-1}. In our spectrum, Fig. 12, the (5,0)←(1,0) transition is in the same position as the experimentally assigned transition (with a rms error of about 0.3 cm^{-1}). The most intense lines in the 2166.0 cm^{-1} region correspond to the R branch of the (2,1)←(0,0) transition and to the R branches of the (4,1)←(1,1), while around 2167.7 cm^{-1} the most intense lines correspond to the P branch of the (1,2)←(0,0) transition. From Table I we note that the errors after reassignment are much poorer than in the case of the (1,2)←(0,0) transition discussed earlier. The transitions in this region are so weak that it is difficult to be able to charge the accuracy of our theoretical intensities, and therefore to propose a firm reassignment based on them.

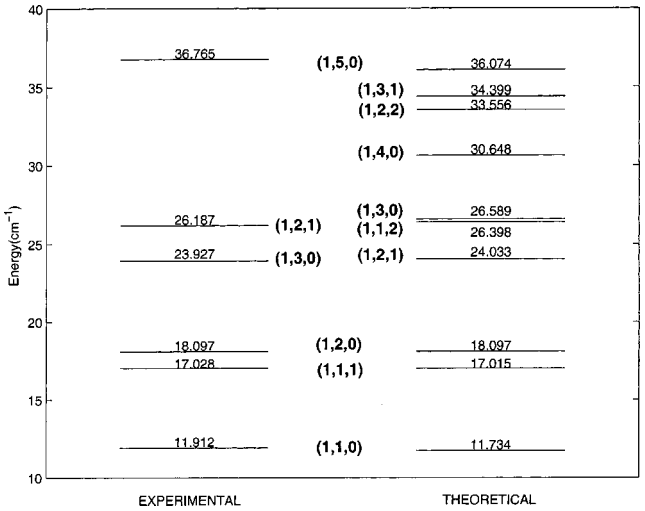

FIG. 14. Comparison between the theoretical and experimental level origins for all the excited van der Waals states up to 37 cm^{-1}. The levels are denoted (ν_{CO},ν_{vdW},K). The experimental states are labeled by the originally assigned quantum numbers.

In the CO fundamental band, according to the theoretical results, the (3,0)←(0,0) transition is located in the 2168–2171 cm^{-1} region.[32] In this region the most intense lines correspond to the P and Q branches of the (3,0)←(0,0) transition (see Fig. 13).

3. The rotational constants

Experimental analysis of rotational constants plays an important role in the prediction of new states[6,10,16] as rotational constants are very sensitive to Coriolis interactions.

Figure 14 shows the experimental (retaining the original assignment) and theoretical results for the "cluster" of three van der Waals levels around 25 cm^{-1} above the $\nu_{CO}=1$ ground state. The analysis of the experimental rotational constants produced a relative level ordering of the close-lying (1,3,0) and (1,1,2) states in contradiction to the theoretical predictions.[10] Later this analysis was revised and the (1,1,2) state was predicted to be close to, but below, the (1,3,0) level,[16] and finally we have suggested that the experimentally assigned (1,2,1) level is actually (1,1,2). As will be shown in the following the Coriolis interaction plays an important role in the analysis of the level ordering of these states.

For $\nu_{CO}=1$ and fixed values of the quantum numbers (ν_{vdW},K) we fit the theoretical rovibrational energies of all the excited van der Waals states up to 40 cm^{-1} to the expression proposed by Hepp *et al.*,[12]

$$E=\sigma+BY-DY^2+HY^3+LY^4\pm\tfrac{1}{2}S, \tag{13}$$

The $-$ sign is chosen for the e components for which $p(-1)^J=+1$, whereas the $+$ sign is used for the f components for which $p(-1)^J=-1$. In Eq. (13), σ is the level origin relative to the van der Waals ground state of the ap-

propriate CO vibrational state, B is the rotational constant, D is the centrifugal distortion constant, etc., and $Y=J(J+1)-K^2$. The asymmetry splitting is given by

$$S=\begin{cases} 0 \quad \text{for } K=0 \\ bZ+dZ[J(J+1)]+hZ[J(J+1)]^2+lZ[J(J+1)]^3 \\ \qquad \text{for } K=1 \\ dZ+hZ[J(J+1)]+lZ[J(J+1)]^2 \quad \text{for } K=2, \end{cases} \tag{14}$$

where $Z=(J+K)!/(J-K)!$.

The rotational constants obtained from the fits are presented in Table II. The strong Coriolis coupling between the (1,2,0) and (1,1,1) states necessitates the use of a different expression in the fitting, such as that of Havenith *et al.*,[6] which takes into account the Coriolis coupling between the *e* components by fitting them simultaneously.

Strong Coriolis interactions in the cluster formed by the (1,2,1), (1,1,2), and (1,3,0) states with $\nu_{CO}=1$ are theoretically predicted. This coupling makes the fitting of these rotational levels to Eq. (13) quite difficult, as reflected by the large rms errors. Hence, each of the components of the states is also fitted separately. The values of the spectroscopic constants obtained from the fits must be considered only as effective values that include the effect of the Coriolis coupling.

To test the effect of the order of the expansion employed in the fitting of the rotational constants, the fits are also performed with an energy expansion that does not include the H and L parameters. The largest changes occur in the rotational constants of the (1,1,2) and (1,3,0) states, reflecting the strong Coriolis perturbation of them both. The large difference between B_e and B_f for the (1,1,2) state shows again the strong perturbation. Although direct Coriolis interaction between the (1,1,2) and (1,3,0) levels is forbidden, an indirect coupling does take place through the (1,2,1) level. In fact, the Coriolis coupling is able to change the ordering of the (1,1,2) and (1,3,0) levels. Before including the off-diagonal Coriolis interaction, the ordering of the level origins of the cluster from lower to higher energy is (1,2,1), (1,3,0), and (1,1,2). After adding the off-diagonal Coriolis terms the (1,1,2) level origin becomes smaller than that of the (1,3,0) level.

IV. SUMMARY AND CONCLUSIONS

Based on the results of a recent study[32] where the rovibrational energy levels of the Ar–CO van der Waals complex were evaluated from a three-dimensional intermolecular potential energy surface obtained with the CCSD(T) method and the aug-cc-pVQZ-33211 basis set, we continue here the evaluation of the spectrum by calculating the three-dimensional electric dipole surface and from there the temperature-dependent spectral intensities. For calculating the dipole surface we use the CCSD method and the aug-cc-pVTZ-33211 basis set.

From the comparison of the calculated absorption spectra with the experimental results, we suggest a reassignment of the (2,1)←(0,2) transition observed around 2160 cm^{-1} to the (1,2)←(0,2). In the case of the (3,0)←(0,0) transition measured around 2166 cm^{-1} the reassignment is less clear because the intensities in this region are very weak, the most intense lines corresponding to the R branch of the (2,1)←(0,0) transition and the P branch of the (1,2)←(0,0) transition. The strong Coriolis interaction between all three van der Waals levels around 25 cm^{-1}, reflected in the effective rotational constants obtained for these levels, is discussed. It is found that the Coriolis coupling is able to change the ordering of the (1,2) and (3,0) states.

ACKNOWLEDGMENTS

The authors acknowledge computer time from DCSC at University of Southern Denmark. This work was supported by the European Research and Training Network ''Molecular Properties and Molecular Materials'' (MOLPROP), Contract No. HPRN-CT-2000-00013, the Spanish Ministerio de Ciencia y Tecnología (PB98-0609-C04-01, BQU2002-02484, and FP99-44446431 FPI grant), and by FEDER (BQU2002-02482).

[1] A. de Piante, E. J. Campbell, and S. J. Buelow, Rev. Sci. Instrum. **60**, 858 (1989).
[2] A. R. W. McKellar, Y. P. Zeng, S. W. Sharpe, C. Wittig, and R. A. Beaudet, J. Mol. Spectrosc. **153**, 475 (1992).
[3] T. Ogata, W. Jäger, I. Ozier, and M. C. L. Gerry, J. Chem. Phys. **98**, 9399 (1993).
[4] M. Havenith, G. Hilpert, M. Petri, and W. Urban, Mol. Phys. **81**, 1003 (1994).
[5] W. Jäger and M. C. L. Gerry, J. Chem. Phys. **102**, 3587 (1995).
[6] S. König, G. Hilpert, and M. Havenith, Mol. Phys. **86**, 1233 (1995).
[7] Y. Xu, S. Civiš, A. R. W. McKellar, S. König, M. Haverlag, G. Hilpert, and M. Havenith, Mol. Phys. **87**, 1071 (1996).
[8] Y. Xu and A. R. W. McKellar, Mol. Phys. **88**, 859 (1996).
[9] M. Hepp, W. Jäger, I. Pak, and G. Winnewisser, J. Mol. Spectrosc. **176**, 58 (1996).
[10] S. König and M. Havenith, Mol. Phys. **91**, 265 (1997).
[11] M. Hepp, R. Gendriesch, I. Pak, F. Lewen, and G. Winnewisser, J. Mol. Spectrosc. **183**, 295 (1997).
[12] M. Hepp, R. Gendriesch, I. Pak, Y. A. Kuritsyn, F. Lewen, G. Winnewisser, M. Brookes, A. R. W. McKellar, J. K. G. Watson, and T. Amano, Mol. Phys. **91**, 229 (1997).
[13] F. Lewen, R. Gendriesch, I. Pak, D. G. Paveliev, M. Hepp, P. Schneider, and G. Winnewisser, Rev. Sci. Instrum. **69**, 32 (1998).
[14] R. Gendreisch, I. Pak, F. Lewen, L. Surin, D. A. Roth, and G. Winnewisser, J. Mol. Spectrosc. **196**, 139 (1999).
[15] A. R. W. McKellar, Mol. Phys. **98**, 111 (2000).
[16] I. Scheele, R. Lehnig, and M. Havenith, Mol. Phys. **99**, 197 (2001).
[17] I. Scheele, R. Lehnig, and M. Havenith, Mol. Phys. **99**, 205 (2001).
[18] D. G. Melnik, S. Gopalakrishnan, T. A. Miller, F. C. D. Lucia, and S. Belov, J. Chem. Phys. **114**, 6100 (2001).
[19] L. A. Surin, B. S. Dumesh, F. Lewen, D. A. Roth, V. P. Kostromin, F. S. Rusin, G. Winnewisser, and I. Pak, Rev. Sci. Instrum. **72**, 2535 (2001).
[20] G. A. Parker and R. T. Pack, J. Chem. Phys. **69**, 3268 (1978).
[21] K. Mirsky, Chem. Phys. **40**, 445 (1980).
[22] J. Tennyson, S. Miller, and B. T. Sutcliffe, J. Chem. Soc., Faraday Trans. 2 **84**, 1295 (1988).
[23] C. A. Parish, J. D. Augspurger, and C. E. Dykstra, J. Phys. Chem. **96**, 2069 (1992).
[24] G. Jansen, Chem. Phys. Lett. **223**, 377 (1994).
[25] V. Castells, N. Halberstadt, S. K. Shin, R. A. Beaudet, and C. Wittig, J. Chem. Phys. **101**, 1006 (1994).
[26] B. Kurkawska-Tarnawska, G. Chałasiński, and K. Olszewski, J. Chem. Phys. **101**, 4964 (1994).
[27] S. Shin, S. K. Shin, and F.-M. Tao, J. Chem. Phys. **104**, 183 (1996).
[28] G. Jansen, J. Chem. Phys. **105**, 89 (1996).
[29] F. A. Gianturco, F. Paesani, M. F. Laranjeira, V. Vassilenko, and M. A. Cunha, J. Chem. Phys. **110**, 7832 (1999).
[30] R. R. Toczyłowski and S. M. Cybulski, J. Chem. Phys. **112**, 4604 (2000).

[31] F. A. Gianturco and F. Paesani, J. Chem. Phys. **115**, 249 (2001).
[32] T. B. Pedersen, J. L. Cacheiro, B. Fernández, and H. Koch, J. Chem. Phys. **117**, 6562 (2002).
[33] J. S. Muenter, J. Mol. Spectrosc. **55**, 490 (1975).
[34] It is intended to make the Ar–CO electric dipole moment surface available via EPAPS.
[35] A. Rizzo, C. Hättig, B. Fernández, and H. Koch, J. Chem. Phys. **117**, 2609 (2002).
[36] T. Helgaker, H. J. Aa. Jensen, P. Jørgensen *et al.*, DALTON, a molecular electronic structure program, Release 1.2, 2001. http://www.kjemi.uio.no/software/dalton/dalton.html
[37] A. Halkier, H. Koch, O. Christiansen, P. Jørgensen, and T. Helgaker, J. Chem. Phys. **107**, 849 (1997).
[38] G. Brocs, J. Tennyson, and A. van der Avoird, J. Chem. Phys. **80**, 3223 (1984).
[39] J. F. Ogilvie, S.-L. Cheah, Y.-P. Lee, and S. P. A. Sauer, Theor. Chem. Acc. **108**, 85 (2002).
[40] P. Huxley and J. N. Murrel, J. Chem. Soc., Faraday Trans. 2 **79**, 323 (1983).
[41] K. Andersson, M. Barysz, A. Bernhardsson *et al.*, MOLCAS, Version 5.2, Lund University, Sweden, 2001. http://www.teokem.lu.se/molcas/
[42] J. Tennyson, S. Miller, and C. R. Le Sueur, Comput. Phys. Commun. **75**, 339 (1993).